Atmos. Chem. Phys. Discuss., 14, 1443–1480, 2014
www.atmos-chem-phys-discuss.net/14/1443/2014/
doi:10.5194/acpd-14-1443-2014

Atmospheric Chemistry and Physics Discussions

One-year observations of size distribution characteristics of major aerosol constituents at a coastal receptor site in Hong Kong – Part 1: Inorganic ions and oxalate

Q. Bian[1,*], **X. H. H. Huang**[2], **and J. Z. Yu**[1,2]

[1]Department of Chemistry, Hong Kong University of Science & Technology, Clear Water Bay, Kowloon, Hong Kong
[2]Institute of the Environment, Hong Kong University of Science & Technology, Clear Water Bay, Kowloon, Hong Kong
[*]now at: Department of Atmospheric Science, Colorado State University, USA

Received: 13 November 2013 – Accepted: 19 December 2013 – Published: 17 January 2014

Correspondence to: J. Z. Yu (jian.yu@ust.hk)

Published by Copernicus Publications on behalf of the European Geosciences Union.

Abstract

Size distribution data of major aerosol constituents are essential in source apportioning of visibility degradation, testing and verification of air quality models incorporating aerosols. We report here one-year observations of mass size distributions of major inorganic ions (sulfate, nitrate, chloride, ammonium, sodium, potassium, magnesium and calcium) and oxalate at a coastal suburban receptor site in Hong Kong, China. A total of 43 sets of size segregated samples in the size range of 0.056–18 µm were collected from March 2011 to February 2012. The size distributions of sulfate, ammonium, potassium and oxalate were characterized by a dominant droplet mode with a mass mean aerodynamic diameter (MMAD) in the range of ~ 0.7–0.9 µm. Oxalate had a slightly larger MMAD than sulfate on days with temperatures above 22 °C as a result of the process of volatilization and repartitioning. Nitrate was mostly dominated by the coarse mode but enhanced presence in fine mode was detected on winter days with lower temperature and lower concentrations of sea salt and soil particles. This data set reveals an inversely proportional relationship between the fraction of nitrate in the fine mode and product of the sum of sodium and calcium in equivalent concentrations and the dissociation constant of ammonium nitrate (i.e., $(1/[Na^+]+2[Ca^{2+}])\times(1/K'_e)$). The seasonal variation observed for sea salt aerosol abundance, with lower values in summer and winter, is possibly linked with the lower marine salinities in these two seasons.

Positive matrix factorization was applied to estimate the relative contributions of local formation and transport to the observed ambient sulfate level through the use of the combined datasets of size-segregated sulfate and select gaseous air pollutants. On average, the regional/super-regional transport of air pollutants was the dominant source at this receptor site, especially on high sulfate days, while local formation processes contributed approximately 30 % of the total sulfate. This work provides field measurement-based evidence for importance of understanding both local photochemistry and regional/super-regional transport in order to properly simulate sulfate aerosols in air quality models.

ACPD
14, 1443–1480, 2014

1 Introduction

Size distribution of aerosols records information of sources and atmospheric processing of particulates. These characteristics of atmospheric particles directly influence local visibility and regional radiative forcing. Substantial knowledge has been gained on the size distributions of the major inorganic ions, elemental carbon (EC) and organic carbon (OC) in the past decade in Hong Kong (HK) and over the adjacent Pearl River Delta (PRD) region in South China (Zhuang et al., 1999a, b; Yao et al., 2003; Huang et al., 2006; Liu et al., 2008; Yu et al., 2010; Lan et al., 2011). The major species, including sulfate, ammonium, OC and EC, predominantly resided in the droplet mode with mass mean aerodynamic diameter (MMAD) in the range of 0.56–1.0 µm over this region while nitrate was often observed to have a dominant presence in the coarse mode (> 3.2 µm) in the coastal areas. In these past studies, however, there is a lack of concurrent measurements of other data (e.g., gaseous data) (Zhuang et al., 1999b; Huang et al., 2006; Yu et al., 2010; Lan et al., 2011) or only a short period was covered, e.g., PRIDE-PRD campaign 2004 and 2006 in summer (Liu et al., 2008; Yue et al., 2010). In this work, integrated and comprehensive observations of gaseous and particulate pollutants were obtained for one-year at the Air Quality Research Supersite (http://envr.ust.hk/research/research-facility/background-materials.html) of the Hong Kong University of Science and Technology (HKUST) by state-of-the-art online instruments and filter-based measurements.

To understand the aerosol formation and processing during the transport through aerosol size distribution measurements is one of the research objectives of the supersite project. Hong Kong is influenced by contrasting air masses in winter and summer due to the Asian monsoon system. The HKUST supersite is located upwind of HK. During most of time in winter the prevailing wind is from north/northeast. In summer, the dominant wind affecting the site is mainly from South China Sea with relatively clean air mass. As such, it is an appropriate place to study the influence of air pollution from outside HK. The size distribution measurements also provide essential data in

ACPD
14, 1443–1480, 2014

evaluating the performance of air quality models and improving its aerosol processing module. The mass scattering efficiency derived from size distribution of aerosols can further provide theoretical validation for source apportionment of visibility reduction. In addition, concurrent online instrument-based and offline filter-based measurements increase confidence of the data reliabilities. As it will be demonstrated later in this paper, the measurements of a number of gaseous and particulate pollutants (e.g. CO, SO_2, O_3, $PM_{2.5}$, etc.) at the same site provide supplementary information for further understanding of aerosol processing. The multiple concurrent measurements conducted at this supersite improve the data utility and data interpretation significantly as compared with those in previous size distribution studies.

Sulfate remains to be among the top contributors to aerosols over the PRD region (He et al., 2011; Huang et al., 2014), although a consensus on SO_2 emission reduction has reached between Hong Kong SAR Government and Guangdong Provincial Government since 2002 http://www.epd.gov.hk/epd/english/environmentinhk/air/prob_solutions/strategies_apc.html#point_1). There is great interest in determining the relative contributions of local formation vs. regional/super-regional transport to sulfate ambient loadings. A number of numerical modeling approaches (e.g. observational based model and source-oriented model) have been applied to identify the source origins of sulfate over this region (Zhang et al., 2009; Wu, 2013; Xue et al., 2014). The accuracy of the results from these numerical studies heavily relies on whether emission inventory and meteorological dynamics are properly represented in the models. In this work we attempt to use field measurements of size-segregated chemical composition data and select gaseous pollutants in couple with receptor modeling to estimate local formation vs. transport contributions.

The primary goal of this paper is to characterize the size distributions of major ions in PM samples collected throughout a year at the supersite. Positive Matrix Factorization (PMF) is then applied to apportion measured size-segregated sulfate into locally formed and regional sources. EC and OC in these size-segregated samples were also

ACPD
14, 1443–1480, 2014

measured. Their size distribution characteristics and the major contributing sources will be reported in a separate paper.

2 Sampling location and chemical analysis

A 10-stage Micro-Orifice Uniform Deposit Impactor (MOUDI, non-rotating version, MSP Corp., Shoreview, MN) aerosol sampler was used to collect size-segregated samples with nominal cut sizes of 18 (inlet), 10.0, 5.6, 3.2, 1.8, 1.00, 0.56, 0.32, 0.18, 0.100, and 0.056 µm. The sampler was located at the HKUST Air Quality Research Supersite (22°20′15.72″ N, 114°16′3.23″ E, Fig. S1). The inlet was ∼ 2 m above roof (∼ 14 m a.s.l.) and the sampler was operated at a flow rate of 30 L min^{-1}. The collection substrates were 47 mm quartz fiber filters, pre-baked at 550 °C overnight before sampling. All the filter samples were stored at −18 °C in a refrigerator before analysis. The sampling was carried out for 24 h from midnight to midnight next day every 12 days from 1 March 2011 to 29 February 2012. An additional 12 sets of samples were collected on an ad-hoc basis to target high-pollution days, including one set in July, three in August, one in September, three in October, one in November, and three in February, respectively. The average gravimetric $PM_{2.5}$ concentration was 25.9 ± 17.6 µg m^{-3} on the sampling days (Huang et al., 2014). Among the 12 ad-hoc samples, one sample was collected on 4 August 2012. On this day, relatively low $PM_{2.5}$ (8.8 µg m^{-3}) was recorded, as the predicted influence by the severe typhoon MuiFa did not happen. The $PM_{2.5}$ concentration for the other 11 ad-hoc samples ranged from 17.6 to 61.8 µg m^{-3}.

The MOUDI samples were analyzed for ionic species. One quarter of each filter substrate was extracted with 3 mL of double de-ionized water in an ultrasonic bath for 30 min and the extract was left at 4 °C in a refrigerator overnight to ensure complete extraction. The extracts were filtered using PTFE syringe filter (0.45 µm, Millipore, Billerica, MA, USA) and then analyzed for ionic species using ion chromatography (IC). The anions (i.e., Cl^-, NO_3^-, SO_4^{2-}, $C_2O_4^{2-}$) were separated using an AS-11 column and a gradient elution solution of NaOH. The cations (i.e., Na^+, NH_4^+, K^+, Mg^{2+}, Ca^{2+}) were

ACPD
14, 1443–1480, 2014

separated using a CS-12A column and methanesulfoinc acid as the elution solution (Yang et al., 2005).

Daily $PM_{2.5}$ sampling was conducted using a mid-volume sampler equipped with 5 sampling channels (SASS, Met One Instrument, OR, USA) in the same period. The collection substrates installed in the 5 channels include one Teflon filter for gravimetric determination of $PM_{2.5}$ mass and element analysis by X-ray fluoresce spectrometry, one nylon filter preceded by a MgO-coated denuder for IC analysis of ionic species, and three pre-baked quartz fibers for EC and OC thermal analysis (Huang et al., 2014).

Criteria gaseous pollutants were measured by various gas analyzers including SO_2 (100A, API Inc.), CO (300A, API Inc.) and O_3 (400E, Teledyne Instruments Inc.) from June 2011 to February 2012. Continuous measurements of inorganic species and their related gas-phase components in the ambient air were provided by a MARGA (Metrohm Applikon, the Netherlands) (Huang et al., 2014). Relative humidity (RH), temperature, wind speed and wind direction were recorded by an automatic weather station installed on a 10 m tower at the site and are shown in Fig. S2.

3 Results and discussion

3.1 Comparison between MOUDI and $PM_{2.5}$ measurement

Ionic species measurements (Cl^-, SO_4^{2-}, NO_3^-, $C_2O_4^{2-}$, Na^+, NH_4^+, K^+, Mg^{2+}, and Ca^{2+}) by MOUDI and by the mid-volume $PM_{2.5}$ sampler were compared in Fig. 1. Concentrations for the ions in individual size bins up to 3.2 µm were added up and compared with those in $PM_{2.5}$. Good correlations were found between the two sets of measurements for SO_4^{2-}, Na^+, and NH_4^+, with $R^2 > 0.90$ and the slopes in the range of 0.9–1.1. The slight underestimations of SO_4^{2-} and NH_4^+ by MOUDI were probably caused by particle bounce and sample handling (Stein et al., 1994; Howell et al., 1998; Chang et al., 2000; Duan et al., 2005). The moderate overestimation of Na^+ by MOUDI was likely due to the larger size cut point (i.e., 3.2 µm) for the MOUDI measurements in

ACPD
14, 1443–1480, 2014

comparison with bulk $PM_{2.5}$ measurements. Na^+ was dominated by the coarse mode (> 2.5 µm) and the amount of Na^+ in the size range of 2.5–3.2 µm could be significant relative to Na^+ in $PM_{2.5}$. For the less abundant species (i.e. $C_2O_4^{2-}$, K^+, and Cl^-), the correlation between the MOUDI ($PM_{3.2}$) and $PM_{2.5}$ measurements were still reasonably good ($R^2 > 0.6$). R^2 values for Mg^{2+} and Ca^{2+} were 0.48 and 0.36, respectively. The weaker correlations than those of SO_4^{2-}, Na^+ and NH_4^+ could be explained by the larger measurement uncertainties as a result of their much lower concentration levels.

Comparison of nitrate between MOUDI and $PM_{2.5}$ measurements indicates under-sampling by MOUDI (Fig. 1), which is an expected result of the semi-volatile nature of nitrate. Volatile loss of particulate nitrate is anticipated due to the pressure drop in the lower 7–10 stages of the MOUDI sampler while such a loss was avoided in the $PM_{2.5}$ sampler as the Nylon filter substrates effectively retain ammonium nitrate. A strong temperature-dependence was also observed in the correlation of nitrate between the two sets of measurements. The correlation in winter ($R^2 = 0.96$, slope = 1.17) was much better than that in summer ($R^2 = 0.13$, slope = −2.58), reflecting the increased dissociation of ammonium nitrate, thereby more volatile loss of nitrate at higher ambient temperatures.

In summary, the comparisons indicate that the MOUDI measurements for the less volatile ionic species are reliable while nitrate measurements by MOUDI were subjected to sampling artifacts due to volatile loss. The under-sampling of nitrate was more significant for summer samples than for the winter samples.

3.2 Size distribution characteristics

Ambient aerosol size distribution is characterized by multiple modes, i.e. nucleation mode, condensation mode, droplet mode and coarse mode, each of which corresponds to distinct aerosol sources and formation pathways. For example, particles in the condensation mode are usually relatively fresh aerosols while the droplet mode

ACPD
14, 1443–1480, 2014

particles may have gone through in-cloud processing and are more likely linked to regional/super-regional transport (Meng and Seinfeld, 1994).

The continuous size distributions were inverted from measurements for the limited number of size bins by adapting the Twomey algorithm on the known response function of the cascade impactor (Twomey, 1975; Winklmayr et al., 1990). Tri-modal log-normal distributions were used to fit the measured data in this work on the assumption that the ambient particle population is superposition of three log-normal modes (i.e., condensation, droplet, and coarse modes) (Dzubay and Hasan, 1990; Dong et al., 2004). The modal concentrations and MMADs are listed in Table 1. The fitted size distributions fall into two groups, one group with a dominant condensation mode (Fig. 2a) and the second group with a prominent coarse mode (Fig. 2b). More details are discussed in the ensuing sections.

3.2.1 Size distributions of NH_4^+, SO_4^{2-}, $C_2O_4^{2-}$ and K^+

The first group of ionic species, including NH_4^+, SO_4^{2-}, $C_2O_4^{2-}$ and K^+, share a common characteristic of a dominant droplet mode (Fig. 2a). The size distribution patterns for SO_4^{2-} and NH_4^+ are very similar, with MMAD of $\sim 0.2\,\mu m$ for the condensation mode, $\sim 0.8\,\mu m$ for the droplet mode, and 4.0–5.0 µm for the coarse mode. The mass distributions of SO_4^{2-} in these three modes were 3.0–5.9 %, 75–81 % and 14–21 %, respectively. The percentages of NH_4^+ were 3.4–4.7 %, 81–89 % and 4.2–16 %, respectively. The molar ratio of $2 \times [SO_4^{2-}]$ and $[NH_4^+]$ in particles of $< 3.2\,\mu m$ ($PM_{3.2}$) was 1.04, indicating that fine sulfate mainly existed in the form of ammonium sulfate.

Air masses influencing HK vary with the shift of synoptic-scale meteorology in PRD from season to season. In this study, the season break-down adopts the definition by Louie et al. (2005), that is, spring is from March to May, summer is from June to August, fall is from September to November, and winter is from December to February. No significant seasonality in size distribution pattern was observed for SO_4^{2-} and NH_4^+.

ACPD
14, 1443–1480, 2014

Sulfate and ammonium were most abundant in the spring, mainly due to the increase of mass concentration in the droplet mode.

$C_2O_4^{2-}$ shows similar size distribution pattern to that of sulfate. The MMADs of the condensation, droplet, and coarse modes were 0.1–0.2, 0.7–0.9 and 4.0–5.0 µm, respectively and the mass percentages were 0–8.1 %, 73–82 % and 18–21 %, respectively. Yu et al. (2005) observed good correlations between ambient oxalate and sulfate measurements across a wide geographical span in East Asia and argued that a common dominant formation pathway, likely in-cloud processing, could explain the close tracking of the two chemically distinct species. For the samples taken in this work, the correlation between the two species in the 0.56–1.0 µm size bin was good (R^2 = 0.69), in agreement with the suggestion of the common in-cloud processing formation process.

It is noted that the MMAD and standard deviation (σ_g) of the droplet mode oxalate in summer were noticeably larger than those of sulfate while the MMAD and σ_g values of the two species were similar in the other seasons. This prompted us to examine the mass concentration ratios of both oxalate and sulfate between the two size bins of 1.0–1.8 µm and 0.56–1.0 µm (Fig. 3). It is clear that the SO_4^{2-} ratio between the two size bins was lower than the $C_2O_4^{2-}$ ratio on sampling days with temperature higher than 22 °C (mostly in summer) while the ratios for the two species were comparable in the other seasons. This result could be explained by evaporation of oxalic acid from the smaller-size particles followed by condensation onto larger particles due to their higher alkalinity. This evaporation-and-re-condensation process was first proposed by Yao et al. (2003) to explain the enhanced presence of oxalate in the size range of 1.0–1.8 µm.

The dominant presence of K^+ in the droplet mode could be explained by that the K^+ containing particles can be easily cloud-activated. The good correlation (R^2 = 0.64) between K^+ and SO_4^{2-} in the size bin of 0.56–1.0 µm supports the suggestion of in-cloud processing. Condensation mode of K^+, accounting for a small fraction (1.1–8.6 %), may be mostly from fresh biomass burning emissions. K^+ in the coarse mode (20–

ACPD
14, 1443–1480, 2014

37 %) might originate from sea salt, soil or the coagulation of small biomass burning particles onto coarse particles.

3.2.2 Size distributions of nitrate, sea salt species, and crustal species

The second group of ionic species, including NO_3^-, Na^+, Cl^-, Ca^{2+}, and Mg^{2+}, share a common size distribution characteristic of a prominent coarse mode (Fig. 2b). Both bimodal (one fine mode and one coarse mode) and tri-modal (i.e., one fine mode and two coarse modes) fitting of the measurement data were carried out. In the case of bimodal lognormal fitting, the Twomey algorithm would result in skewed log-normal distribution curves (Fig. S3). On the other hand, tri-modal data fitting is able to capture the measured size distributions with three log-normally distrusted particle populations (Fig. 2b). The inverted size distributions for this group of species are therefore represented with one fine and two coarse modes. The underlying physical basis for the presence of two coarse modes will be discussed in detail in the later section.

The droplet mode MMAD values for all five species ranged from 0.8–1.5 µm. The MMAD of the smaller coarse mode (I) ranged from 3.0–4.2 µm and the larger coarse mode (II) ranged from 6.8–8.1 µm for sea salt species (Na^+, Mg^{2+}, and Cl^-). Andreas (1998) summarized that sea spray droplets fall into three types and their respective size ranges are film droplets (0.5–5 µm), jet droplets (3–50 µm) and spume droplets (> 20 µm). Film droplets are ejected due to the rupturing of film-thin top of oceanic bubbles on the surface of sea; jet bubbles are formed from the bottom of surface bubbles after their burst; and spume droplets are produced when the wind tears sea water right off the wave crests. The two coarse modes retrieved for the sea salt species likely correspond to film droplets and jet droplets. Sea salt particles of spume droplets are not expected to be captured by MOUDI sampling as this sampler only collects particles up to 18 µm. And this sea salt particle formation theory also explained the small amount of sea salt in the droplet mode (< 2.5 µm).

The mass concentration of sea salt aerosol was averagely lower in the summer and winter than in the spring and fall (Table 1). Wai and Tanner (2004) suggested that sea

ACPD
14, 1443–1480, 2014

salt particle concentration is closely dependent on wind speed and seawater salinity. The wind speed at the site was lower in the summer while the speed in the winter was similar to those in the spring and fall (Fig. S2). Thus, the wind speed was unlikely a dominant factor affecting the concentration of sea salt aerosols at the sampling site. Thiyagarajan et al. (2002) reported that salinity in eastern HK was the highest (34 ‰) in spring, the next highest (32 ‰) in fall while lower (30 ‰) in the summer and winter. The lower salinity around HK waters in summer and winter is due to input of fresh water plumes from the Pearl River and the Yangtze River, respectively (Guan and Fang, 2006; Gan et al., 2009). It is plausible that the higher salinity of sea water in spring and fall explained the higher abundance of the sea salt ionic species in the atmosphere. Current regional air quality models only consider the influence of wind speed and RH on the sea salt concentration in the coastal surf zone (Kelly et al., 2010). Our results suggest that the oceanic salinity may need to be considered in the parameterization in sea salt emissions in air quality models.

Soluble Ca^{2+} is the product of soil component (i.e., calcium carbonate) reacting with acidic gases (e.g., HNO_3) or co-existing acidic aerosol components (e.g., H_2SO_4, HSO_4^-). The larger coarse mode (MMAD: 7.0–7.7 µm) accounted for a dominant fraction (55–77 %), the smaller coarse mode (MMAD: 3.1–4.0 µm) accounted for 21–37 %, and a minor fraction (2–12 %) was in the fine mode (Table 1). The smaller coarse mode Ca^{2+} is likely associated with long-range transported dust particles while the larger coarse mode is mainly associated with locally-produced soil particles. Such a differentiation of two coarse mode dust particles with respect to different source origins was previously suggested by Husar (2004) and VanCuren et al. (2005). Ca^{2+} in the fine and in the smaller coarse mode was found to correlate strongly with Si in the collocated $PM_{2.5}$ samples (R^2 = 0.54 and 0.80, respectively) (Fig. 4) while Ca^{2+} in the large coarse mode had a much weaker correlation with Si in $PM_{2.5}$ (R^2 = 0.24). This result further supports the hypothesis that the smaller coarse mode Ca^{2+} might be associated with long-range transported dust particles. The mass concentration of Ca^{2+} in spring was ~ 1.4–2.2 times higher than those in other seasons, indicating the increased influ-

ACPD
14, 1443–1480, 2014

ence of dust transported from the North China Plain on HK in this season (Lee et al., 2010).

Nitrate is closely associated with sea salt and dust particles as a result of its formation process through the reactions of acidic HNO_3 gas with alkaline components (e.g., Harrison and Poi, 1983). Fitting the measured nitrate size distributions with three log-normal distributions produces a droplet mode of MMAD in the range of 0.8–1.0 µm (2–13 %), coarse mode I of MMAD in the range of 3.0–4.2 µm (22–47 %), and coarse mode II of MMAD in the range of 6.8–7.4 µm (41–62 %). Unlike other ionic species, the relative abundances of nitrate in different size modes are highly variable among the seasons. The average percentage of aerosol nitrate in the fine mode (< 1.8 µm), denoted as P_{n_fine} thereafter, was significantly higher in the winter samples (37 %) than those in the spring (13 %), summer and fall (≤ 6 %).

3.2.3 Factors affecting fine mode nitrate

Fine mode nitrate is mainly in the form of NH_4NO_3 while the coarse mode nitrate is the product of heterogeneous reaction between gaseous NO_2 or HNO_3 and alkaline species such as Ca^{2+} and Na^+ (Pakkanen et al., 1996; Yoshizu and Hoshi, 1985). NH_4NO_3 is a thermally unstable species and its abundance in aerosols is governed by the following thermodynamic equilibrium.

$$NH_4NO_3(s, aq) \leftrightarrow HNO_3(g) + NH_3(g) \quad \text{(R1)}$$

The amount of aerosol NH_4NO_3 is dependent on RH, temperature (T), and concentrations of gas-phase nitric acid and ammonia (Mozurkewich, 1993). Under the RH conditions at the sampling site (normally larger than 80 % during the sampling period) (Fig. S2), calculations using the thermodynamic equilibrium model (i.e. ISORROPIA) show that the nitrate particles were in the liquid status.

The dissociation constant (K_e) is inherently dependent on RH and T. In addition, ionic strength of the aerosol liquid phase also influences the gas-particle partitioning of NH_4NO_3. For instance, coexistence of SO_4^{2-} in particles reduces K_e in the

ACPD
14, 1443–1480, 2014

$NH_4^+/NO_3^-/SO_4^{2-}$ system and helps to retain nitrate in the aerosol phase (Stelson and Seinfeld, 1982; Seinfeld and Pandis, 2006). For this reason, a modified dissociation constant K_e' is introduced to take into consideration of the ionic strength effect. K_e' is defined to be the product of K_e and Y, where Y is $[NH_4NO_3]/([NH_4NO_3]+3[(NH_4)_2SO_4]$. Our calculations showed that K_e' varied from 0.06 to 5.1 ppb^2 for individual samples and was less than 1.5 ppb^2 for most of the samples collected in spring and winter (Fig. S4). The plot of K_e' vs. P_{n_fine} (Fig. 5a) shows a clear inverse relationship between the two variables, and P_{n_fine} is significant (> 10 %) only when K_e' falls below 1.0 ppb^2.

Due to the tendency of gaseous HNO_3/N_2O_5 reacting with alkaline sea salt and soil particles (Reactions R2–R4) (Yao and Zhang, 2012), the alkaline species compete for gaseous HNO_3 and thus the abundance of the alkaline species is expected to affect the amount of NH_4NO_3 partitioning onto the fine particles,

$$NaCl(s) + HNO_3(g) \rightarrow NaNO_3(s) + HCl(g)\uparrow \quad (R2)$$

$$NaCl(s) + N_2O_5(g) \rightarrow NaNO_3(s) + ClNO_2(g)\uparrow \quad (R3)$$

$$CaCO_3(s) + 2HNO_3(g) \rightarrow Ca(NO_3)_2(s) + H_2O + CO_2(g)\uparrow \quad (R4)$$

The sum of the two major ions (Na^+ and Ca^{2+}) (in equivalent concentrations) is indicative of the abundance of alkaline species on sea salt and soil particles. It is plotted against P_{n_fine} in Fig. 5a and a clear inverse relationship is observed. The coarse mode equivalent concentration of Na^+ and Ca^{2+} was the highest (above 0.2 $\mu eq\,m^{-3}$) in spring (Fig. S4), which explains the less significant presence of fine mode nitrate in samples collected in spring than those in winter. The following empirical relationship is found between P_{n_fine} and the product of $(1/K_e')$ and $(1/[Na^+]+2[Ca^{2+}])$ (Fig. 5b):

$$P_{n\_fine} = 0.006 \times \left(\frac{1}{K_e'}\right) \times \left(\frac{1}{[Na^+]+2[Ca^{2+}]}\right) + 0.069, R^2 = 0.73 \quad (1)$$

This result clearly indicates that in coastal environments, sea salt plays an active role in modulating the amount of nitrate residing in the fine mode particles.

ACPD
14, 1443–1480, 2014

3.2.4 Relationship of coarse mode nitrate formation and chloride depletion

Coarse mode nitrate formation and chloride depletion on sea salt particles are closely linked through Reaction (R2). The percentages of the chloride depleted ($Cl^-_{depletion}$ %) for size bins larger than 3.2 µm were calculated and summarized in Table 2. Generally, the extent of Cl^- depletion is progressively higher on relatively smaller particles, which is an expected result of more abundant acidic species on the smaller particles. The equivalent ratios of $([Cl^-] + [NO_3^-])/[Na^+]$ on coarse particles ranged from 1.20–1.88, which were close to the $[Cl^-]/[Na^+]$ ratio in sea water (1.174). It is suggested by Yao and Zhang (2012) that this similarity indicates that the overall chloride depletion could be largely explained by the coarse mode nitrate formation. MARGA data also showed that the measured HNO_3(g) and HCl(g) were moderately correlated in the regime of low P_{n_fine} (percentage of fine mode nitrate < 30 %) (Fig. S5), supporting R2 as a significant pathway for Cl^- depletion.

3.2.5 Comparison of size distributions of secondary ionic species with previous studies

Table S1 lists the measurements of MMAD of SO_4^{2-}, NO_3^-, NH_4^+ and $C_2O_4^{2-}$ at the HKUST site in the past decades. MMAD of the condensation mode slightly increased from ~ 0.2 µm in 1996 (Zhuang et al., 199b) to ~ 0.3 µm in 2008 (Yu et al., 2010) and in this study. The MMAD of the droplet mode for sulfate increased from ~ 0.6 µm in 1996 to 0.8–0.9 µm in 2008 and 2011–2012 (this study). It is difficult to discern whether this observation of shift of the droplet mode to a large size was incidental (due to the limited measurements and the low temporal resolution in the MOUDI measurements) or reflected increased contributions of sulfate via regional transport in the recent measurement periods. SO_4^{2-} was neutralized by gaseous NH_3 in the atmosphere and NH_4^+ thus has the similar variation of size distribution as SO_4^{2-} (Zhuang et al., 1999b; Louie et al., 2005a).

ACPD
14, 1443–1480, 2014

In winter of 1996–1997, coarse-mode nitrate was dominant, with a MMAD of 3.95 µm while in the winter of 2008 and in 2011–2012, nitrate exhibited bimodal distributions. The fine mode nitrate concentration was 0.58, 1.01 and 1.43 $\mu g\,m^{-3}$ in the three periods, respectively. The average concentration of the gaseous precursor (NO_x) was ~ 7.7 ppb in the winter of 1999 and 2000, ~ 13.8 ppb in the winter of 2008 and ~ 10.3 ppb in this study, respectively. The increasing concentration level of NO_x would lead to higher local production of HNO_3. It is likely that alkaline species were insufficient to neutralize the increased HNO_3 or NO_3^- and thus a larger proportion of HNO_3 partitions to the fine particles.

No oxalate concentration was reported in the dataset of 1996–1997. MMADs in the condensation mode, droplet mode and coarse mode of this species were comparable in 2008 and 2011–2012.

3.3 PMF analysis of size-segregated sulfate with selected gaseous pollutants

Multivariate receptor modeling has been widely used to identify underlying emission sources and formation processes and to estimate source contributions to measured ambient particulate concentration. Several studies have succeeded in applying factor analytic algorithms (Positive Matrix Factorization (PMF) and Multilinear Engine (ME-2)) to size distribution measurements to retrieve source contribution on the assumption of a unique size distribution for each contributing source and linearity between particle number and mass concentration over time at a fixed site (Kim et al., 2004; Zhou et al., 2004, 2005). In the following analysis, PMF approach was adopted to estimate the relative contributions of local formation and regional/superregional transport to the observed ambient sulfate.

3.3.1 PMF analysis of size-segregated sulfate

The 43 sets of size-segregated sulfate concentrations were combined with the gaseous pollutant measurements (CO, SO_2 and O_x) for PMF analysis using EPA PMF3.0. SO_2

ACPD
14, 1443–1480, 2014

is the gaseous precursor of particulate sulfate. O_x (the sum of NO_2 and O_3) is usually used to evaluate the oxidation capability of ambient atmosphere. CO is generally considered as an anthropogenic combustion tracer. No obvious combustion sources are found in the vicinity of the sampling location to the best of our knowledge while the CO concentrations were observed to be higher in winter and lower in summer (Fig. S6). This is consistent with the seasonal pattern of pollutants transported from outside HK to this site. Therefore, CO is used as a tracer for transported pollutants in this study.

The minimum sample size (N) needed for obtaining statistically reliable results by factor analysis is $30 + (V + 3)/2$, where V is the number of input species (Henry et al., 1984). In order to reduce the input variables, data from adjacent size bins were grouped together, reducing the input size-segregated data to the following five size categories: (1) 0.056–0.32 µm; (2) 0.32–0.56 µm; (3) 0.56–1.0 µm; (4) 1.0–3.2 µm; and (5) > 3.2 µm. The dataset of 8 measured variables ×43 samples was then organized as input matrix for PMF analysis. Uncertainty prepared for PMF analysis was set as the sum of analytical uncertainty and 1/3 of detection limit for lumped sulfate species (Reff et al., 2007) and 30 % of the corresponding concentration for CO, SO_2 and O_x. Three to five factors were tested in PMF analysis and the three-factor solution was found to best explain the sulfate formation. In the four- and five- factor solutions, sulfate in the size category of 1.0–3.2 µm forms a factor without association with any gas tracers, leaving this factor unexplained. Five different seed values were tested and similar results were obtained. The seed value was eventually set at 123. Bootstrapping on the base solution reported stable results, with > 85 out of 100 bootstrap factors mapped with those in the based run. Positive F_{peak} values were applied to sharpen the F matrix and to achieve cleaner source profiles. Q values as a function of F_{peak} values are plotted in Fig. S7. Source profile shows the application of F_{peak} of 0.1 gives the best result.

The first factor consists of all sulfate in the size range of 0.056 to 0.32 µm, 72 % of sulfate in the size bin of 0.32–0.56 µm, 48 % of SO_2 and 66 % of O_x. Particles in the size bin of 0.056–0.32 µm are associated with the condensation process. The abundant presence of sulfate in this size bin indicates that this factor is associated with

ACPD
14, 1443–1480, 2014

freshly formed aerosols. Reaction of SO_2 with OH radical was the major pathway of sulfate formation in the gas phase while H_2O_2 is the dominant oxidant for SO_2 oxidation in the aqueous phase (Seinfeld and Pandis, 2006; Miyakawa et al., 2007). The ratio ($[SO_4^{2-}]/([SO_2]+[SO_4^{2-}])$) is calculated to be 0.30, close to the sulfate conversion extent near power plant sources (Wilson, 1981). This further supports the association of this factor with the freshly formed sulfate particles.

The second factor accounts for more than 60 % of sulfate in the size from 0.56 to 3.2 µm and nearly 100 % of CO. The conversion factor of SO_2 to sulfate in this factor is 0.97, much larger than that in the first factor. These characteristics indicate that this factor is associated with aged sulfate, i.e., sulfate transported from outside HK.

Nearly all of particulate sulfate on particles > 3.2 µm appeared in the third factor. This factor is therefore identified as sulfate in the coarse mode and its further apportionment to different sources/formation pathways is discussed in the next section.

The sum of apportioned sulfate well explains the ambient sulfate measurements (Fig. 7a). The seasonal average contributions from the three PMF-resolved sources are plotted in Fig. 7b. Locally-formed sulfate ranged from 0.11 to 6.7 $\mu g\,m^{-3}$ in individual samples with the higher values occurring in the spring and fall (~ 3.0 $\mu g\,m^{-3}$), consistent with the high oxidant potential (O_x) during these two seasons (Fig. S6). Transported sulfate was in the range of 0.10–17 $\mu g\,m^{-3}$ in individual samples with the highest seasonal average occurring in spring. Seasonal average sulfate in the coarse mode ranged from 0.3–1.3 $\mu g\,m^{-3}$ with the highest value in spring. The annual average contribution was estimated to be 30 % (2.5 $\mu g\,m^{-3}$) associated with local oxidation of SO_2, 59 % (4.9 $\mu g\,m^{-3}$) due to sulfate transported from outside HK, and 11 % (0.9 $\mu g\,m^{-3}$) sulfate in the coarse mode. In the high sulfate cases (total $[SO_4^{2-}] > 14.4\,\mu g\,m^{-3}$, the value corresponding to average + one standard variation of the whole data set), the regional/super-regional pollutant transport played a key role, accounting for an average of 68 % of total sulfate and 78 % of sulfate in fine mode.

ACPD
14, 1443–1480, 2014

3.3.2 PMF analysis of coarse-mode sulfate

To further understand the formation pathway and sources of sulfate in the coarse mode, sulfate and other ionic species (Na^+, Mg^{2+}, NO_3^-, Ca^{2+}, K^+ and NH_4^+) in the coarse mode were organized as input matrix for PMF analysis. $PM_{2.5}$ Si as a tracer for bulk soil particles (no coarse Si data available) was also included as input data, as its inclusion significantly improves the agreement of PMF-reconstructed and measured Ca^{2+} data. Uncertainties for these variables were set as the sum of analytical uncertainty and 1/3 of detection limit. Four factors were found to reasonably explain the physical meaning of each source (Fig. 8).

Prominent Na^+, Mg^{2+}, K^+, Cl^- and ~ 13 % of the coarse-mode sulfate appear in the first factor. Na^+, Mg^{2+} and some of K^+ on particles larger than 3.2 µm are considered to be the tracers for sea salt particles. Major ions in sea water with salinity of 35 ‰ are Cl^- (55.29 % in the mass percentage), Na^+ (30.74 %), Mg^{2+} (3.69 %), SO_4^{2-} (7.75 %), Ca^{2+} (1.18 %) and K^+ (1.14 %) (Millero and Sohn, 1992). The relative abundance of individual species resolved by PMF in this factor agreed fairly well with that in the sea water except that the PMF-derived SO_4^{2-} was about half of that in the sea water (Fig. S8). This factor therefore was identified as fresh sea salt.

The second factor consists of 98 % of NH_4^+, 64 % of SO_4^{2-}, 23 % of NO_3^-, 13 % Na^+, and 11 % of Si. The equivalent ratio of NH_4^+, SO_4^{2-}, and NO_3^- (1.5 : 1.0 : 1.0) in this factor indicates that sulfate mainly exist as NH_4HSO_4 and nitrate as NH_4NO_3. Coarse mode sulfate apportioned to this factor (termed as $[SO_4^{2-}]_{C\_F2}$ hereafter) could be due to co-agulation of fine NH_4HSO_4 and NH_4NO_3 particles with coarse sea salt/dust particles or re-suspension of dust particles that contain NH_4HSO_4 and NH_4NO_3, the presence of which in dust could come from dry or wet deposition of ambient aerosols. As Ca^{2+} in the smaller coarse mode (i.e., $[Ca^{2+}]_{CMI}$) represents long-range transported dust particles, an association between $[SO_4^{2-}]_{C\_F2}$ and $[Ca^{2+}]_{CMI}$ is anticipated if coagulation of NH_4HSO_4 fine particles is a significant source for $[SO_4^{2-}]_{C\_F2}$. On the other hand,

ACPD
14, 1443–1480, 2014

an association between $[SO_4^{2-}]_{C\_F2}$ and Ca^{2+} in coarse mode II (i.e., $[Ca^{2+}]_{CMII}$) is expected if re-suspension of dust particles is a significant source for $[SO_4^{2-}]_{C\_F2}$. We next examine correlations of $[SO_4^{2-}]_{C\_F2}$ with $[Ca^{2+}]_{CMI}$ and $[Ca^{2+}]_{CMII}$. It is found that the samples fall into two groups. For samples with lower $[SO_4^{2-}]_{C\_F2}$ (roughly $< 0.4\,\mu g\,m^{-3}$, $n = 28$), $[SO_4^{2-}]_{C\_F2}$ strongly correlates with $[Ca^{2+}]_{CMI}$ ($R^2 = 0.68$) (Fig. 9b) while the correlation with $[Ca^{2+}]_{CMII}$ is significantly weaker ($R^2 = 0.49$). For samples with higher $[SO_4^{2-}]_{C\_F2}$ (roughly $> 0.5\,\mu g\,m^{-3}$, $n = 13$), on the other hand, a moderate positive correlation ($R^2 = 0.53$, Fig. 9b) exists between $[SO_4^{2-}]_{C\_F2}$ and $[Ca^{2+}]_{CMII}$ while the correlation with $[Ca^{2+}]_{CMI}$ is much weaker ($R^2 = 0.23$). The correlation results indicate that both the coagulation process and re-suspended dust particles could be significant sources for $[SO_4^{2-}]_{C\_F2}$. That PMF failed to resolve these two sources is most likely due to the limited number of sample size.

The third factor is characterized by abundant presence of nitrate, Ca^{2+}, and chloride-depleted sea salt species (Na^+, Mg^{2+}, and K^+). This factor thus was identified as the mixture of aged sea salt and dust particles.

The fourth factor is identified as fresh dust particles that have not undergone atmospheric processing (such as acidification), as this factor is characterized with abundant Si and Ca^{2+} but little sulfate and absence of nitrate.

The comparisons of PMF-reconstructed and measured coarse mode concentrations show R^2 values of linear regression better than 0.95 for NO_3^-, Cl^-, NH_4^+, Na^+, and Mg^{2+}, and 0.83 for Ca^{2+} (Table S2). The agreement for coarse sulfate ($R^2 = 0.79$) is weaker but still reasonable (Fig. 9a). This result indicates that the PMF solution captures most of the variation in the coarse-mode sulfate while it also suggests that likely there are sources or processes not properly represented by the input species. The small sample size and lack of direct coarse dust particle tracer data may be the contributing causes for the limitation in the PMF solution for the coarse sulfate.

ACPD
14, 1443–1480, 2014

The PMF results show that on average two-thirds of coarse sulfate is NH_4HSO_4-containing coarse particles ($\sim 0.5\,\mu g\,m^{-3}$) while the other three sources (i.e., sea salt sulfate, dust sulfate, and aged sea salt/dust particles) make comparable contributions to the remaining one-third coarse sulfate.

4 Summary and implications

Size distributions of nine ionic species (SO_4^{2-}, NO_3^-, Cl^-, $C_2O_4^{2-}$, Na^+, NH_4^+, K^+, Mg^{2+}, and Ca^{2+}) were determined in a total of 43 sets of samples collected at a suburban receptor location over a year. SO_4^{2-}, NH_4^+, $C_2O_4^{2-}$ and K^+ mainly resided in the droplet mode with MMAD of 0.7–0.9 µm. Minor volatilization and repartition of $C_2O_4^{2-}$ led to a larger MMAD and a broader size distribution for the droplet mode under conditions of higher temperatures (i.e. over 22 °C). Two coarse modes and one droplet mode were inverted for the species associated with sea salt and dust particles, with MMADs of the two coarse modes as 2–4 µm and 6–8 µm, respectively. The smaller coarse mode for Ca^{2+} was likely associated with long-range transported dust particles while the larger coarse mode is mainly associated with locally-produced soil particles. The seasonal variation of ambient sea salt concentrations could be caused by the seasonal fluctuation in the marine salinity. Modifications of the parameterization in sea salt emission and the oceanic salinity in the air quality models are needed in order to improve the model performance.

As a result of interacting with sea salt and dust particles, NO_3^- was generally dominated by the coarse mode. Enhanced presence of nitrate in fine mode was observed on winter days of lower temperature and on days with lower concentrations of sea salt and soil particles. An inversely proportional relationship was established using the data set between the fraction of nitrate in the fine mode and $(1/[Na^+] + 2[Ca^{2+}]) \times (1/K'_e)$, i.e., product of the sum of alkaline ions in equivalent concentrations (Na^+ and Ca^{2+})

ACPD
14, 1443–1480, 2014

and the modified dissociation constant of ammonium nitrate. This relationship explains the variable characteristics in nitrate size distribution.

Local formation and transport contribution of sulfate were estimated by applying PMF analysis on the combined datasets of size-segregated sulfate and select gaseous air pollutants (SO_2, O_x and CO). The regional/super-regional source dominated the observed sulfate at HKUST, especially on high sulfate days. On average, the regional source contributed 59 % (4.9 $\mu g\,m^{-3}$) while the locally-formed sulfate accounted for 30 % (2.5 $\mu g\,m^{-3}$), and the remaining sulfate (0.9 $\mu g\,m^{-3}$) was on coarse mode particles. Further PMF analysis of the coarse mode chemical composition data suggests that most of the coarse-mode sulfate were contributed by NH_4HSO_4-containing coarse particles. This source of coarse sulfate has its origin in fine NH_4HSO_4 particles, which is shifted to the coarse mode through coagulation and/or deposition followed by resuspension. Results from this study demonstrate the importance of understanding both local photochemistry and regional/super-regional transport in order to properly model sulfate aerosols.

Supplementary material related to this article is available online at http://www.atmos-chem-phys-discuss.net/14/1443/2014/acpd-14-1443-2014-supplement.pdf.

Acknowledgements. This work was supported by the Environmental Conservation Funds (ECF) of Hong Kong (ECWW09EG04). We thank Hong Kong Environmental Protection Department for making available the MARGA data and Alexis Lau for the criteria gas monitoring data. Bian Q. also thanks Liu Zhiqiang for valuable discussion of possible factors driving atmospheric sea salt particulate variability in Hong Kong.

ACPD
14, 1443–1480, 2014

References

Andreas, E. L.: A new sea spray generation function for wind speeds up to 32 m s^{-1}, J. Phys. Oceanogr., 28, 2175–2184, 1998.

Chang, M. C., Sioutas, C., Kim, S., Gong, H., and Linn, W. S.: Reduction of nitrate losses from filter and impactor samplers by means of concentration enrichment, Atmos. Environ., 34, 85–98, 2000.

Dong, Y., Hays, M. D., Smith, N. D., and Kinsey, J. S.: Inverting cascade imparctor data for size-resolved characterization of fine partculate source emissions, J. Aerosol Sci., 35, 1497–1512, 2004.

Duan, J. C., Bi, X. H., Tan, J. H., Sheng, G. Y., and Fu, J. M.: The differences of the size distribution of polycyclic aromatic hydrocarbons (PAHs) between urban and rural sites of Guangzhou, China, Atmos. Res., 78, 190–203, 2005.

Dzubay, T. G. and Hasan, H.: Fitting multimodal lognormal size distributions to Cascade Impactor data, Aerosol Sci. Tech., 13, 144–150, 1990.

Gan, J. P., Cheung, A., Guo, X. G., and Li, L.: Intensified upwelling over a widened shelf in the northeastern South China Sea, J. Geophys. Res., 114, C09019, doi:10.1029/2007JC004660, 2009.

Guan, B. X. and Fang, G. H.: Winter counter-wind currents off the southeastern China coast: a review, J. Oceanogr., 62, 1–24, 2006.

Harrison, R. M. and Pio, C. A.: Size-cifferentiated composition of inorganic atmospheric aerosols of both marine and polluted continental origin, Atmos. Environ., 17, 1733–1738, 1983.

Henry, R. C., Lewis, C. W., and Hopke, P. K., Williamson, H. J.: Review of receptor model fundamentals, Atmos. Environ., 18, 1507–1515, 1984.

Howell, S., Pszenny, A. A. P., Quinn, P., and Huebert, B.: A field intercomparison of three cascade impactors, Aerosol Sci. Tech., 29, 475–492, 1998.

He, L.-Y., Huang, X.-F., Xue, L., Hu, M., Lin, Y., Zheng, J., Zhang, R., and Zhang, Y.-H.: Submicron aerosol analysis and organic source apportionment in an urban atmosphere in Pearl River Delta of China using high-resolution aerosol mass spectrometry, J. Geophys. Res.-Atmos., 116, D12304, doi:10.1029/2010JD014566, 2011.

ACPD
14, 1443–1480, 2014

Huang, X. H. H., Bian, Q., Ng, W. M., Louie, P. K. K., and Yu, J. Z.: Characterization of $PM_{2.5}$ major components and source investigation in suburban Hong Kong: a one year monitoring study, Aerosol Air Qual. Res., in press, 2014.

Huang, X. F., Yu, J. Z., He, L. Y., and Yuan, Z. B.: Water-soluble organic carbon and oxalate in aerosols at a coastal urban site in China: size distribution characteristics, sources, and formation mechanisms, J. Geophys. Res.-Atmos., 111, D22212, doi:10.1029/2006JD007408, 2006.

Huar, R. B.: Intercontinental Transport of Dust: Historical and Recent Observational Evidence, Springer Verlag, chap. 11, 2004.

Kelly, J. T., Bhave, P. V., Nolte, C. G., Shankar, U., and Foley, K. M.: Simulating emission and chemical evolution of coarse sea-salt particles in the Community Multiscale Air Quality (CMAQ) model, Geosci. Model Dev., 3, 257–273, doi:10.5194/gmd-3-257-2010, 2010.

Kim, E., Hopke, P. K., Larson, T. V., and Covert, D. S.: Analysis of ambient particle size distributions using unmix and positive matrix factorization, Environ. Sci. Technol., 38, 202–209, 2004.

Lan, Z. J., Chen, D. L., Li, X., Huang, X. F., He, L. Y., Deng, Y. G., Feng, N., and Hu, M.: Modal characteristics of carbonaceous aerosol size distribution in an urban atmosphere of South China, Atmos. Res., 100, 51–60, 2011.

Lee, Y. C., Yang, X., and Wenig, M.: Transport of dusts from East Asian and non-East Asian sources to Hong Kong during dust storm related events 1996–2007, Atmos. Environ., 44, 3728–3738, 2010.

Liu, S., Hu, M., Slanina, S., He, L. Y., Niu, Y. W., Bruegemann, E., Gnauk, T., and Herrmann, H.: Size distribution and source analysis of ionic compositions of aerosols in polluted periods at Xinken in Pearl River Delta (PRD) of China, Atmos. Environ., 42, 6284–6295, 2008.

Louie, P. K. K., Wastson, J. G., Chow, J. C., Chen, A., Sin, D. W. M., and Lau, A. K. H.: Seasonal characteristics and regional transport of $PM_{2.5}$ in Hong Kong, Atmos. Environ., 29, 1695–1710, 2005.

Meng, Z. Y. and Seifeld, J. H.: On the source of the submicrometer droplet mode of urban and regional aerosols, Aerosol Sci. Tech., 20, 253–265, 1994.

Millero, F. J. and Sohn, M. J., Chemistry Oceanography, CRC Press, Boca Raton, FL, 1992.

Miyakawa, T., Takegawa, N., and Kondo, Y.: Removal of sulfur dioxide and formation of sulfate aerosol in Tokyo, J. Geophys. Res.-Atmos., 112, D13209, doi:10.1029/2006JD007896, 2007.

ACPD
14, 1443–1480, 2014

Mozurkewich, M.: The dissociation-constant of ammonium-nitrate and its dependence on temperature, relative-humidity and particle-size, Atmos. Environ., 27, 261–270, 1993.
Pakkanen, T. A., Kerminen, V. M., Hillamo, R. E., Makinen, M., Makela, T., and Virkkula, A.: Distribution of nitrate over sea-salt and soil derived particles – implications from a field study, J. Atmos. Chem., 24, 189–205, 1996.
Reff, A., Eberly, S. I., and Bhave, P. V.: Receptor modeling of ambient particulate matter data using positive matrix factorization: review of existing methods, J. Air Waste Manage., 57, 146–154, 2007.
Seinfeld, J. H. and Pandis, S. N.: Atmospheric Chemistry and Physics – from Air Pollution to Climate Change, 2nd edn., John Wiley & Sons, USA, p. 311, p. 477, 2006.
Stein, S. W., Turpin, B. J., Cai, X. P., Huang, C. P. F., and Mcmurry, P. H.: Measurements of relative humidity-dependent bounce and density for atmospheric particles using the DMA-impactor technique, Atmos. Environ., 28, 1739–1746, 1994.
Stelson, A. W. and Seinfeld, J. H., Thermodynamic prediction of the water activity, NH_4NO_3 dissociation-constant, density and refractive-index for the NH_4NO_3–$(NH_4)_2SO_4$–H_2O-system at 25 °C, Atmos. Environ., 16, 2507–2514, 1982.
Thiyagarajan, V., Harder, T., and Qian, P. Y.: Effect of the physiological condition of cyprids and laboratory-mimicked seasonal conditions on the metamorphic successes of Balanus amphitrite Darwin (Cirripedia; Thoracica), J. Exp. Mar. Biol. Ecol., 274, 65–74, 2002.
Twomey, S.: Comparison of constrained linear inversion and an iterative nonlinear algorithm applied to indirect estimation of particle-size distributions, J. Comput. Phys., 18, 188–200, 1975.
VanCuren, R. A., Cliff, S. S., Perry, K. D., and Jimenez-Cruz, M.: Asian continental aerosol persistence above the marine boundary layer over the eastern North Pacific: continuous aerosol measurements from Intercontinental Transport and Chemical Transformation 2002 (ITCT 2K2), J. Geophys. Res.-Atmos., 110, D09S90, doi:10.1029/2004JD004973, 2005.
Wai, K. M. and Tanner, P. A.: Wind-dependent sea salt aerosol in a Western Pacific coastal area, Atmos. Environ., 38, 1167–1171, 2004.
Wilson, W. E.: Sulfate formation in point source plumes: a review of recent field studies, Atmos. Environ., 15, 2573–2581, 1981.
Winklmayr, W., Wang, H. C., and John, W.: Adaptation of the twomey algorithm to the inversion of cascade impactor data, Aerosol Sci. Tech., 13, 322–331, 1990.

ACPD
14, 1443–1480, 2014

Wu, D.: Numerical study of atmospheric particulate matters: source apportionment to characterize 3D transport and transformation of precursors and secondary pollutants, Ph. D. thesis, Hong Kong University of Science & Technology, 2013.
Xue, J., Yuan, Z., Yu, J. Z., and Lau, A. K. H.: An observation-based model for secondary inorganic aerosols, Aerosol Air Qual. Res., in press, 2014.
Yang, H., Yu, J. Z., Ho, S. S. S., Xu, J., Wu, W.-S., Wan, C. H., Wang, X., Wang, X., and Wang, L., The chemical compostion of inorganic and carbonaceous materials in $PM_{2.5}$ in Nanjing, China, Atmos. Environ., 39, 3735–2749, 2005.
Yao, X. H. and Zhang, L. M.: Chemical processes in sea-salt chloride depletion observed at a Canadian rural coastal site, Atmos. Environ.46, 189–194, 2012.
Yao, X. H., Fang, M., and Chan, C. K.: The size dependence of chloride depletion in fine and coarse sea-salt particles, Atmos. Environ., 37, 743–751, 2003.
Yoshizumi, K. and Hoshi, A.: Size distributions of ammonium-nitrate and sodium-nitrate in atmospheric aerosols, Environ. Sci. Technol., 19, 258–261, 1985.
Yu, H., Wu, C., Wu, D., and Yu, J. Z.: Size distributions of elemental carbon and its contribution to light extinction in urban and rural locations in the pearl river delta region, China, Atmos. Chem. Phys., 10, 5107–5119, doi:10.5194/acp-10-5107-2010, 2010.
Yu, J. Z., Huang, X. F., Xu, J. H., and Hu, M.: When aerosol sulfate goes up, so does oxalate: implication for the formation mechanisms of oxalate, Environ. Sci. Technol., 39, 128–133, 2005.
Yue, D. L., Hu, M., Wu, Z. J., Guo, S., Wen, M. T., Nowak, A., Wehner, B., Wiedensohler, A., Takegawa, N., Kondo, Y., Wang, X. S., Li, Y. P., Zeng, L. M., and Zhang, Y. H.: Variation of particle number size distributions and chemical compositions at the urban and downwind regional sites in the Pearl River Delta during summertime pollution episodes, Atmos. Chem. Phys., 10, 9431–9439, doi:10.5194/acp-10-9431-2010, 2010.
Zhang, H., Li, J., Ying, Q., Yu, J. Z., Wu, D., Cheng, Y., He, K., and Jiang, J.: Source apportionment of $PM_{2.5}$ nitrate and sulfate in China using a source-oriented chemical transport model, Atmos. Environ., 62, 228–242, 2012.
Zhou, L., Kim, E., Hopke, P. K., Stainier, C., and Pandis, S. N.: Advanced factor analysis on Pittsburgh particle size distribution data, Aerosol Sci. Tech., 38, 118–132, 2004.
Zhou, L., Hopke, P. K., Stainer, C. O., Pandis, S. N., Ondov, J. M., and Pancras, J. P.: Investigation of the relationship between chemical composition and size distribution of airborne

ACPD
14, 1443–1480, 2014

particles by partial least squares and positive matrix factorization, J. Geophys. Res.-Atmos., 110, D07S18, doi:10.1029/2004JD005050, 2005.

Zhuang, H., Chan, C. K., Fang, M., and Wexler, A. S.: Formation of nitrate and non-sea-salt sulfate on coarse particles, Atmos. Environ., 33, 4223–4233, 1999a.

Zhuang, H., Chan, C. K., Fang, M., and Wexler, A. S.: Size distributions of particulate sulfate, nitrate, and ammonium at a coastal site in Hong Kong, Atmos. Environ., 33, 843–853, 1999b.

ACPD
14, 1443–1480, 2014

Table 1a. Mass mean aerodynamic diameters (MMAD, μm), standard deviation (σ_g) and modal concentrations of ionic species (C_m, $\mu g\,m^{-3}$) in spring (N = 8, N represent number of samples), summer (N = 11), fall (N = 13) and winter (N = 11).

	Condensation mode			Droplet mode			Coarse mode		
	C_m ($\mu g\,m^{-3}$)	MMAD (μm)	σ_g	C_m ($\mu g\,m^{-3}$)	MMAD (μm)	σ_g	C_m ($\mu g\,m^{-3}$)	MMAD (μm)	σ_g
SO_4^{2-}									
*Spring	0.59	0.24	1.31	9.51	0.84	1.51	2.64	5.07	2.07
Summer	0.32	0.25	1.34	5.30	0.83	1.54	0.91	5.13	2.06
Fall	0.56	0.28	1.30	7.30	0.80	1.38	1.63	4.38	2.31
Winter	0.26	0.26	1.25	6.78	0.84	1.50	1.62	5.03	2.16
NH_4^+									
Spring	0.26	0.24	1.38	3.79	0.82	1.49	0.63	4.92	2.14
Summer	0.14	0.26	1.35	1.94	0.82	1.53	0.09	5.02	2.35
Fall	0.23	0.30	1.30	2.64	0.78	1.36	0.20	4.25	2.51
Winter	0.12	0.26	1.26	2.86	0.84	1.50	0.56	5.06	2.17
K^+									
Spring	0.03	0.22	2.18	0.23	0.81	1.49	0.10	5.09	2.05
Summer	0.00	0.16	2.17	0.12	0.78	1.63	0.07	5.73	1.77
Fall	0.01	0.28	1.25	0.22	0.81	1.46	0.08	5.89	1.81
Winter	0.02	0.28	1.27	0.34	0.79	1.49	0.09	4.70	2.16
$C_2O_4^{2-}$									
Spring	0.02	0.22	1.35	0.30	0.80	1.66	0.08	4.58	1.81
Summer	0.00	0.12	1.51	0.18	0.92	2.02	0.04	5.25	1.64
Fall	0.03	0.11	2.59	0.27	0.84	1.66	0.07	4.83	1.81
Winter	0.01	0.29	1.28	0.21	0.77	1.49	0.06	4.58	2.12

* Spring is defined as the period from March to May, summer is from June to August, fall is from September to November, and winter is from December to February.

ACPD
14, 1443–1480, 2014

Table 1b. Mass mean aerodynamic diameters (MMAD, μm), standard deviation (σ_g) and modal concentrations of ionic species (C_m, $\mu g\,m^{-3}$) in spring (N = 8, N represent number of samples), summer (N = 11), fall (N = 13) and winter (N = 11).

	Droplet mode			Coarse mode I			Coarse mode II		
	C_m ($\mu g\,m^{-3}$)	MMAD (μm)	σ_g	C_m ($\mu g\,m^{-3}$)	MMAD (μm)	σ_g	C_m ($\mu g\,m^{-3}$)	MMAD (μm)	σ_g
NO_3^-									
Spring	0.74	0.91	1.55	2.28	4.18	1.42	2.50	7.38	1.24
Summer	0.09	0.77	2.18	0.44	3.40	1.49	0.87	7.19	1.42
Fall	0.14	1.03	2.61	1.47	4.03	1.45	1.54	7.33	1.25
Winter	1.43	0.88	1.44	0.84	2.96	1.53	1.56	6.83	1.44
Na^+									
Spring	0.43	0.90	2.06	1.00	4.07	1.43	1.36	7.49	1.28
Summer	0.14	1.21	1.61	0.66	3.62	1.51	0.95	7.37	1.35
Fall	0.16	1.17	1.61	0.72	3.48	1.51	1.45	7.64	1.32
Winter	0.11	1.10	1.73	0.22	3.40	1.38	0.85	7.67	1.39
Mg^{2+}									
Spring	0.01	1.24	1.45	0.11	3.32	1.50	0.22	6.92	1.39
Summer	0.01	1.15	1.54	0.06	3.09	1.51	0.15	7.06	1.47
Fall	0.01	1.28	1.54	0.08	3.25	1.53	0.18	7.62	1.33
Winter	0.01	1.11	1.57	0.03	3.15	1.51	0.11	7.62	1.45
Ca^{2+}									
Spring	0.11	1.04	2.12	0.27	3.44	1.45	0.50	6.99	1.40
Summer	0.01	1.14	1.50	0.09	3.11	1.45	0.33	7.68	1.47
Fall	0.04	0.85	1.35	0.16	3.96	1.51	0.24	7.59	1.28
Winter	0.02	1.16	1.81	0.10	3.34	1.43	0.33	7.53	1.44
Cl^-									
Spring	0.09	1.35	1.87	0.26	3.84	1.26	1.67	7.76	1.28
Summer	0.04	1.48	1.76	0.81	3.89	1.46	1.34	7.49	1.32
Fall	0.04	1.59	1.52	0.24	3.56	1.25	1.96	7.89	1.33
Winter	0.05	1.27	1.79	0.10	3.37	1.25	1.01	8.09	1.39

ACPD
14, 1443–1480, 2014

Table 2. The percentage of Cl depleted in aged sea-salt aerosols ($Cl^-_{depletion}$ %), relative acidity, and ionic ratios in each season.

	3.2–5.6 µm	5.6–10 µm	10–18 µm	> 18 µm
Spring				
[a]$Cl^-_{depletion}$ %	68.73	42.82	34.58	39.34
[b]Relative acidity	1.42	1.26	1.28	1.30
$([Cl^-]+[NO_3^-])/[Na^+]$	1.26	1.38	1.35	1.21
Summer				
$Cl^-_{depletion}$ %	53.76	34.57	28.28	30.81
Relative acidity	1.22	1.21	1.33	1.41
$([Cl^-]+[NO_3^-])/[Na^+]$	1.20	1.36	1.39	1.34
Fall				
$Cl^-_{depletion}$ %	51.04	28.49	18.50	6.27
Relative acidity	1.05	1.07	1.00	1.06
$([Cl^-]+[NO_3^-])/[Na^+]$	1.20	1.29	1.34	1.42
Winter				
$Cl^-_{depletion}$ %	47.24	29.06	18.81	29.67
Relative acidity	1.16	1.15	1.16	1.17
$([Cl^-]+[NO_3^-])/[Na^+]$	1.88	1.53	1.55	1.41

[a] $Cl^-_{depletion}$ % = $(1.174[Na^+]-[Cl^-])/1.174[Na^+]\times 100$ %.

[b] Relative acidity = $([NH_4^+]+[Na^+]+[Ca^{2+}]+[Mg^{2+}]+[K^+]/([SO_4^{2-}]+[NO_3^-]+[Cl^-])$.

ACPD
14, 1443–1480, 2014

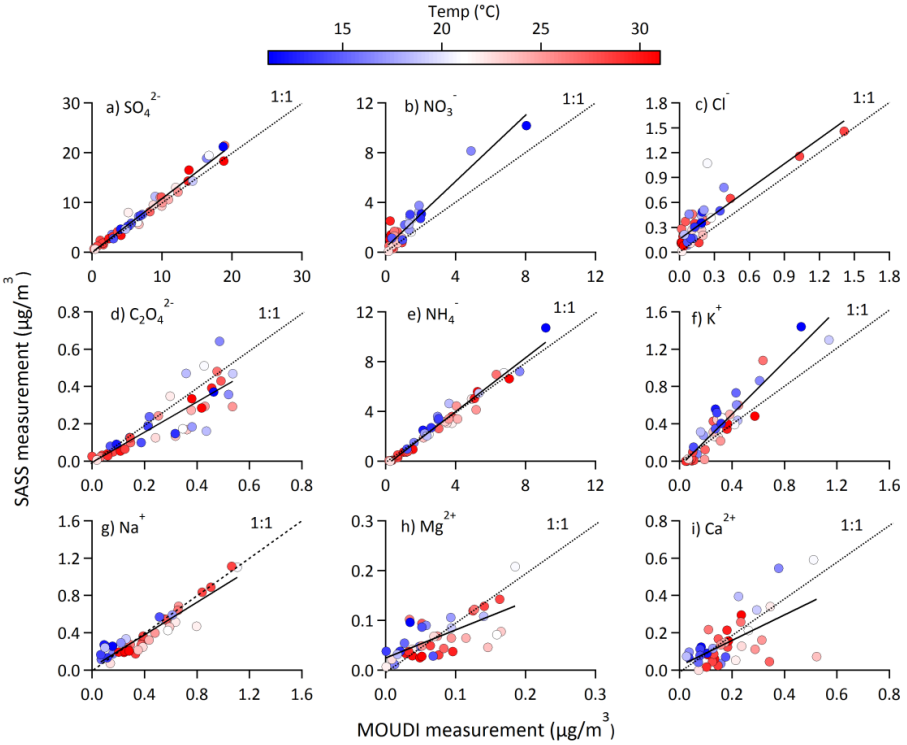

Fig. 1. Comparison between MOUDI measurements (< 3.2 μm) and $PM_{2.5}$ measurements by SASS sampler. Data points are color-coded by ambient temperatures on the individual sampling days. A segregation of data points by temperature was observed for nitrate, see text for details.

ACPD
14, 1443–1480, 2014

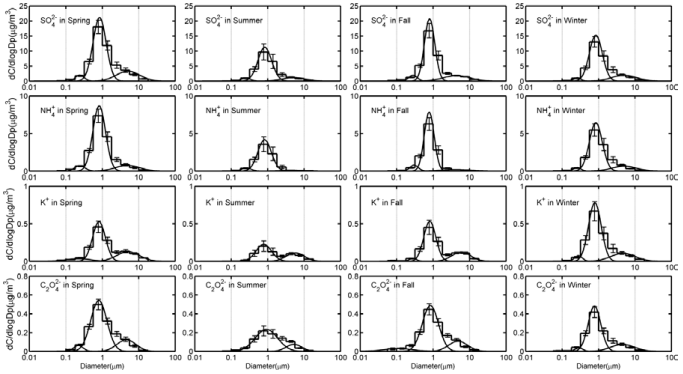

(a)

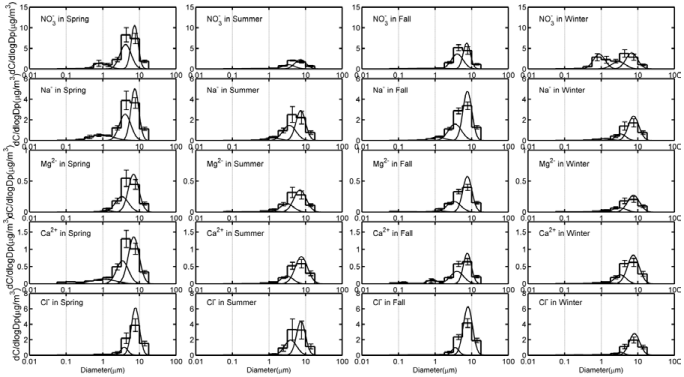

(b)

Fig. 2. Continuous log-normal size distributions of **(a)** species associated with in-cloud processing (SO_4^{2-}, NH_4^+, K^+, $C_2O_4^{2-}$) and **(b)** species associated with crustal and sea salt particles (NO_3^-, Na^+, Mg^{2+}, Ca^{2+}, Cl^-) in the four seasons. The size distributions are inverted from measured MOUDI data, which are shown in histograms.

ACPD
14, 1443–1480, 2014

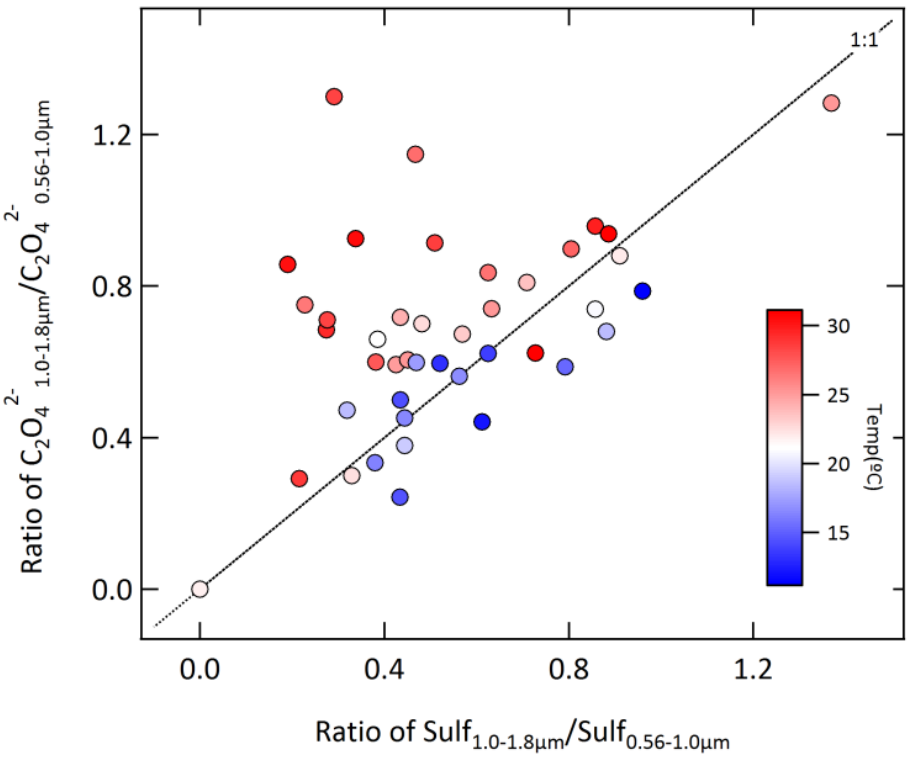

Fig. 3. Comparison of mass concentration ratios of oxalate and sulfate between the two size bins 1.0–1.8 µm and 0.56–1.0 µm. The data points are color-coded according to ambient temperature during their collection.

ACPD
14, 1443–1480, 2014

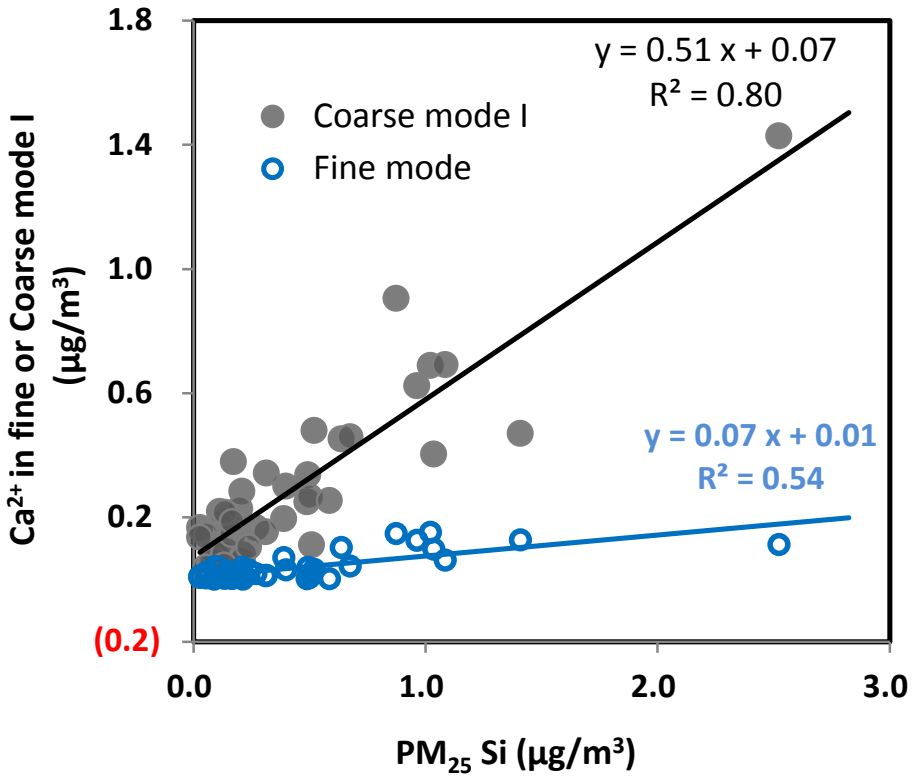

Fig. 4. Correlations of Ca^{2+} in fine mode and coarse mode I with Si in collocated $PM_{2.5}$ samples.

ACPD
14, 1443–1480, 2014

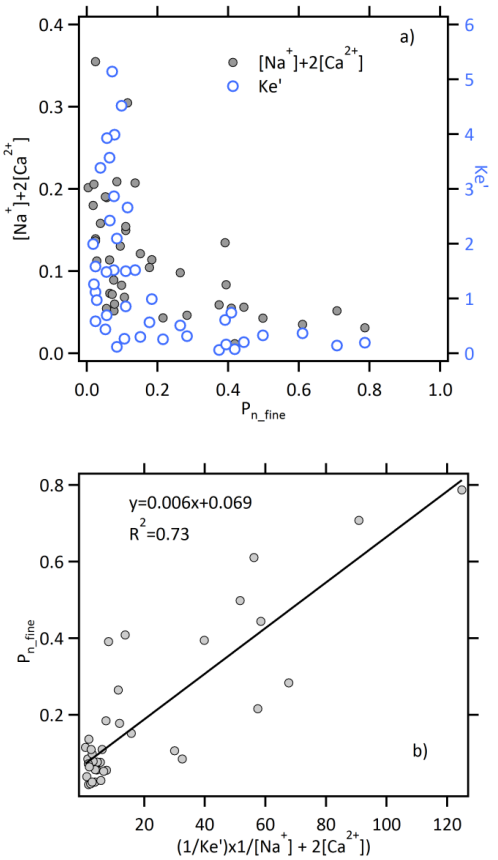

Fig. 5. (a) Relationships of aerosol nitrate fraction in the fine mode (P_{n_fine}) (< 1.8 µm) with modified NH_4NO_3 dissociation equilibrium constant (K'_e) and equivalent amounts of $[Na^+] + 2[Ca^{2+}]$ in the size range of > 3.2µm; **(b)** Empirical relationship between P_{n_fine} and $(1/K'_e) \times 1/([Na^+] + 2[Ca^{2+}])$.

ACPD
14, 1443–1480, 2014

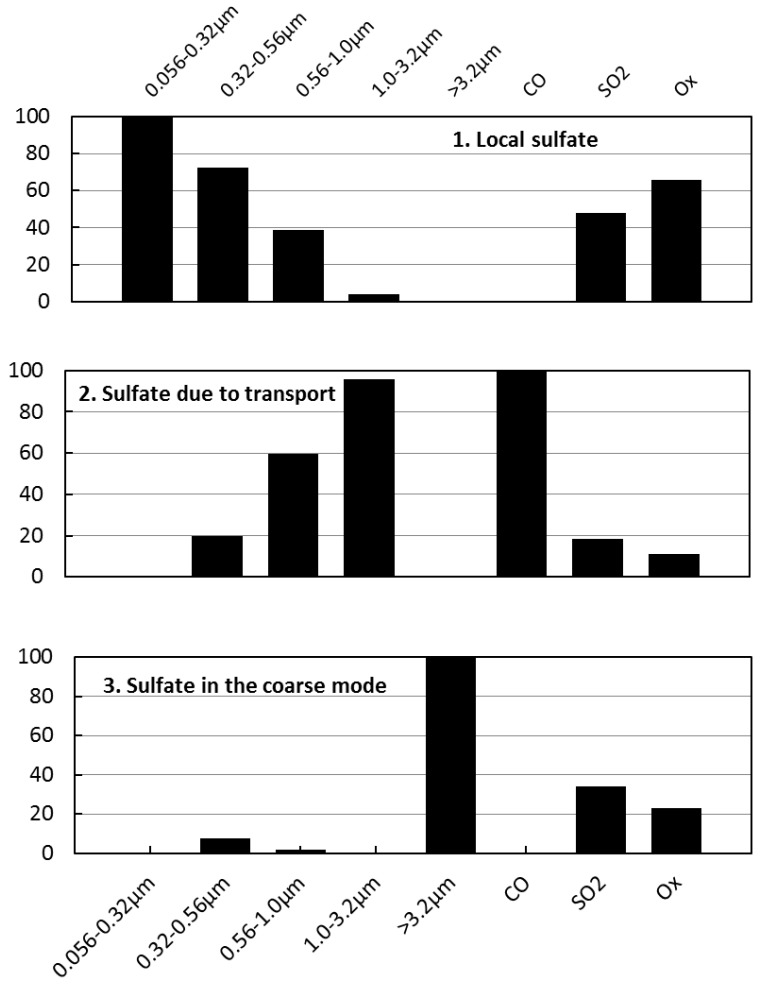

Fig. 6. PMF-resolved source profiles (% of total species) for size-segregated SO_4^{2-}.

ACPD
14, 1443–1480, 2014

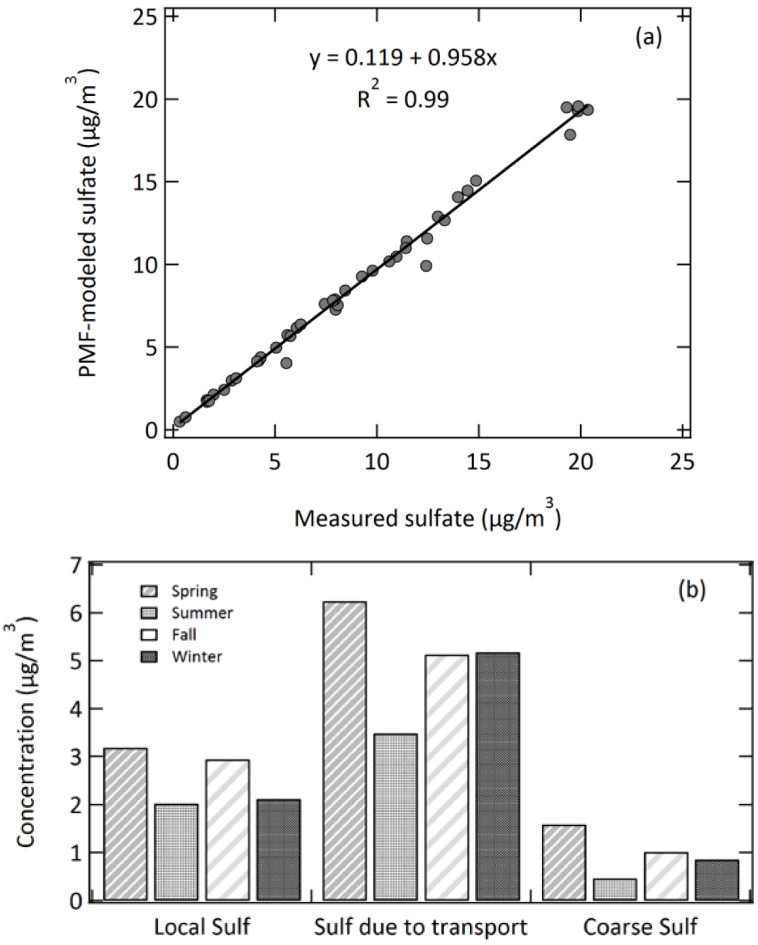

Fig. 7. (a) Comparison of PMF-modeled sulfate with the measured sulfate; **(b)** Seasonal variation in contributions of the three sources to sulfate.

ACPD
14, 1443–1480, 2014

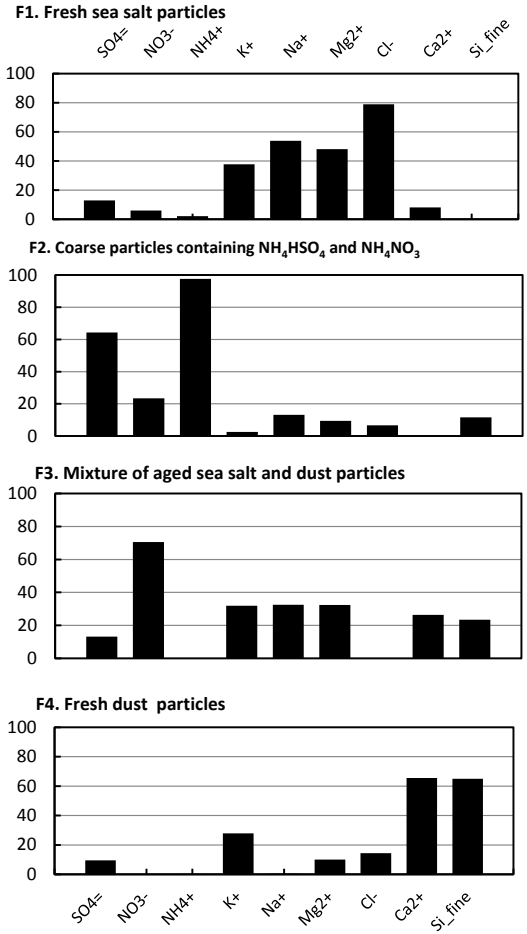

Fig. 8. PMF-resolved source profiles (% of total species) for coarse-mode data. $PM_{2.5}$ Si as a surrogate for bulk dust particles is also included as input data.

ACPD
14, 1443–1480, 2014

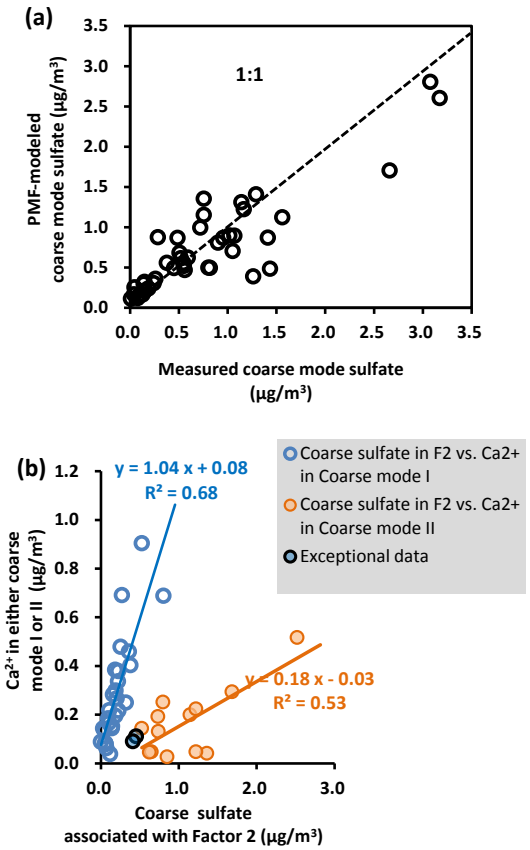

Fig. 9. (a) Total sulfate in the coarse mode vs. PMF-model estimated sulfate. **(b)** Relationship of coarse-mode sulfate apportioned to the NH_4HSO_4-containing coarse particles (i.e., Factor 2) with Ca^{2+} concentration in either Coarse-mode I (blue open circles) or Coarse mode II (yellow filled circles). There are two exceptional data (filled circles with blank outline) that do not fit in either of the two groups.

ACPD
14, 1443–1480, 2014